Supplementary Material

for

Communication and quorum sensing in non-living mimics of eukaryotic cells

Henrike Niederholtmeyer, Cynthia Chaggan, and Neal K. Devaraj

Department of Chemistry and Biochemistry, University of California, San Diego, USA

Correspondence to: ndevaraj@ucsd.edu

Supplementary Figures S1-S15
Supplementary Tables S1-S2
Movies 1-3

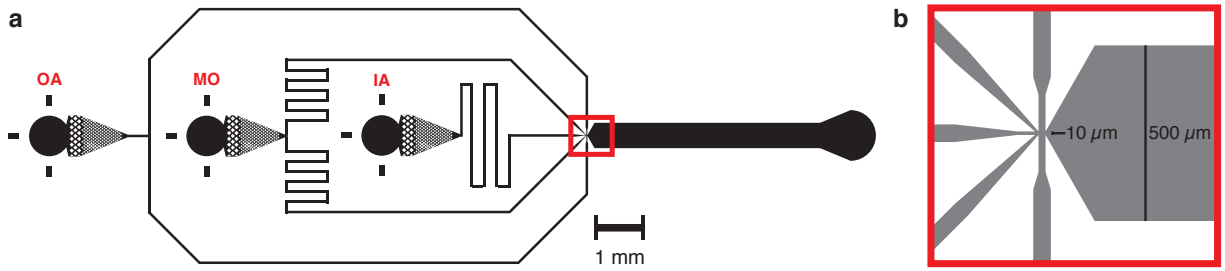

Supplementary Figure S1. Design of the microfluidic device.
a) Design of the microfluidic device used to produce cell-mimics. Inlets for the outer aqueous (OA), middle organic (MO) and inner aqueous phases (IA) are labeled. A magnified view of the flow focusing junction (red box) is shown in b). At the fluidic junction the width of the IA channel is 10 μm.

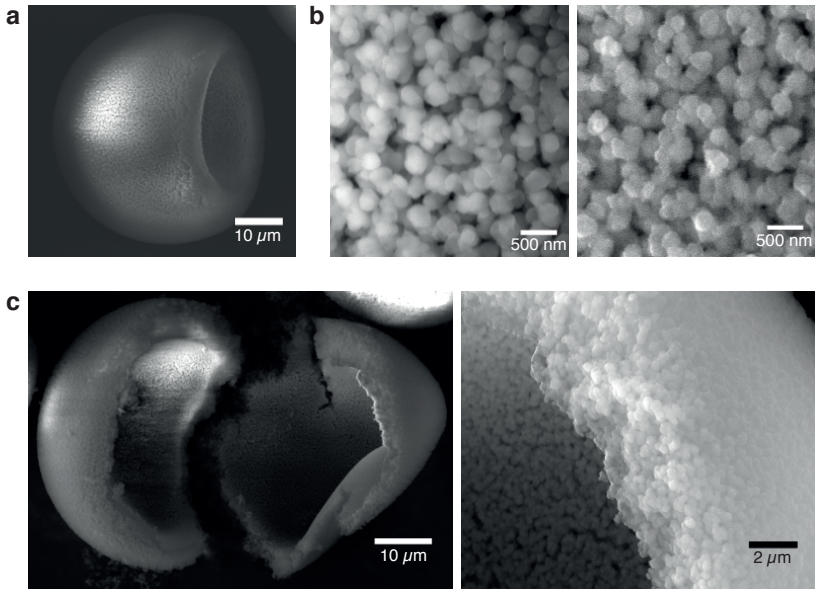

Supplementary Figure S2. Scanning electron microscopy of porous polymer membrane of cell-mimics.
a) Low magnification image of cell-mimic with an indentation. Polymer membranes partly collapsed when cell-mimics dried, which caused indentations in the membrane. b) High magnification images of exterior of microcapsule membranes from two separate batches of cell-mimics. c) Low magnification image of a cracked cell-mimic and magnification of the polymer membrane cross-section.

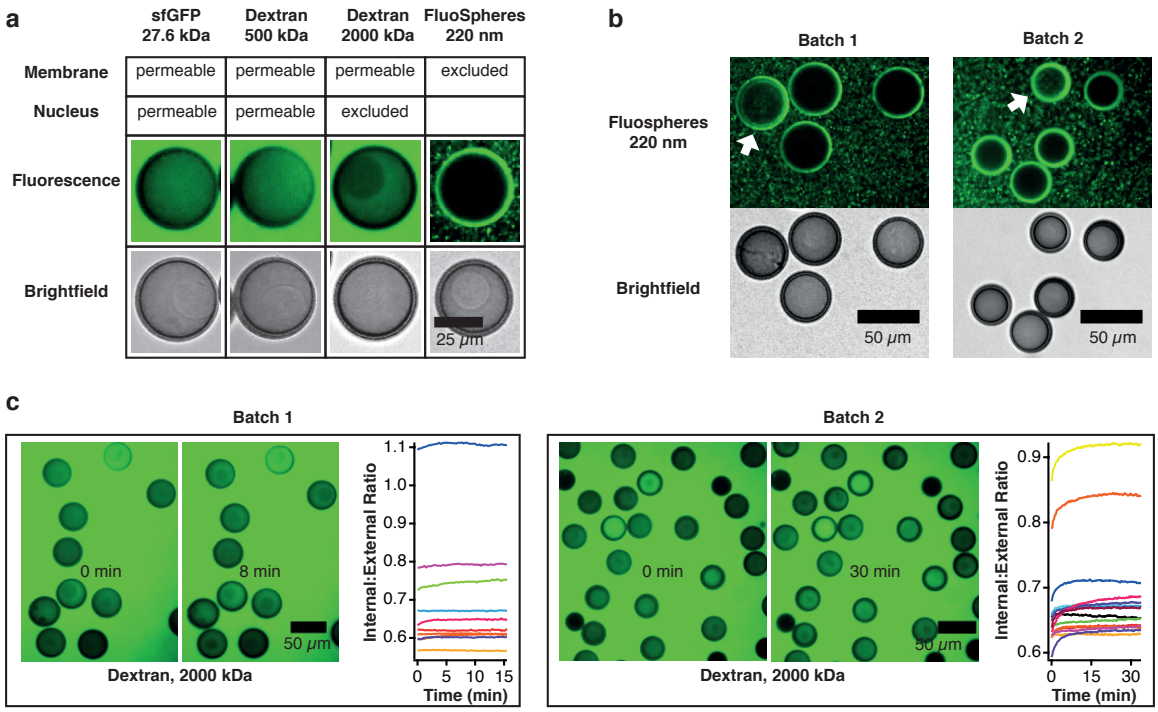

Supplementary Figure S3. Permeability of cell-mimic membranes and clay-DNA hydrogel nuclei.

a) Spinning disk confocal fluorescence images of individual cell-mimics incubated for 24 h with fluorescent tracer molecules of different sizes (top) and corresponding brightfield images (bottom). b) Cell-mimics after incubation with a solution of 220 nm FluoSpheres (Thermo Fisher Scientific). FluoSpheres nanoparticles were excluded from 90% of cell-mimics (n=77, batch 1; n=152, batch 2). Arrows indicate cell-mimics with FluoSpheres in their interior. Many of the cell-mimics with nanoparticles in their interior had visible defects (see brightfield image, batch 1). Images of cell-mimics in a) and b) were acquired after 24 h incubation with labeled tracer molecules in 100 mM HEPES, 0.4% Tween 20. Dextrans were Fluorescein conjugates (Nanocs). c) Diffusion of 2000 kDa dextran into cell-mimics. At time 0, labeled 2000 kDa dextran was added and mixed with cell-mimics in 100 mM HEPES, 0.4% Tween 20. Images were acquired every 15 seconds to monitor diffusion of dextran into the interior of cell-mimics. Fluorescence images show a population of cell- at time 0 and after equilibration of fluorescence signals for cell-mimic batches 1 and 2. Graphs show traces of internal to external fluorescence ratios for individual cell-mimics tracked over time in the shown images. Diffusion of dextran into cell-mimics in batch 2 was slightly slower than for batch 1. An increase in fluorescence could be observed in most batch 2 cell-mimics, while in batch 1, fluorescence levels had already equilibrated at the start of imaging. Final fluorescence intensities varied from cell-mimic to cell-mimic probably because their polymer shells absorbed light to different extends. We observed similar differences in final intensities between cell-mimics for smaller the fluorescent tracer molecules sfGFP and 500 kDa dextran as well. The saturating fluorescence traces show that internal and external 2000 kDa dextran concentrations were equilibrated after 15 min at the latest.

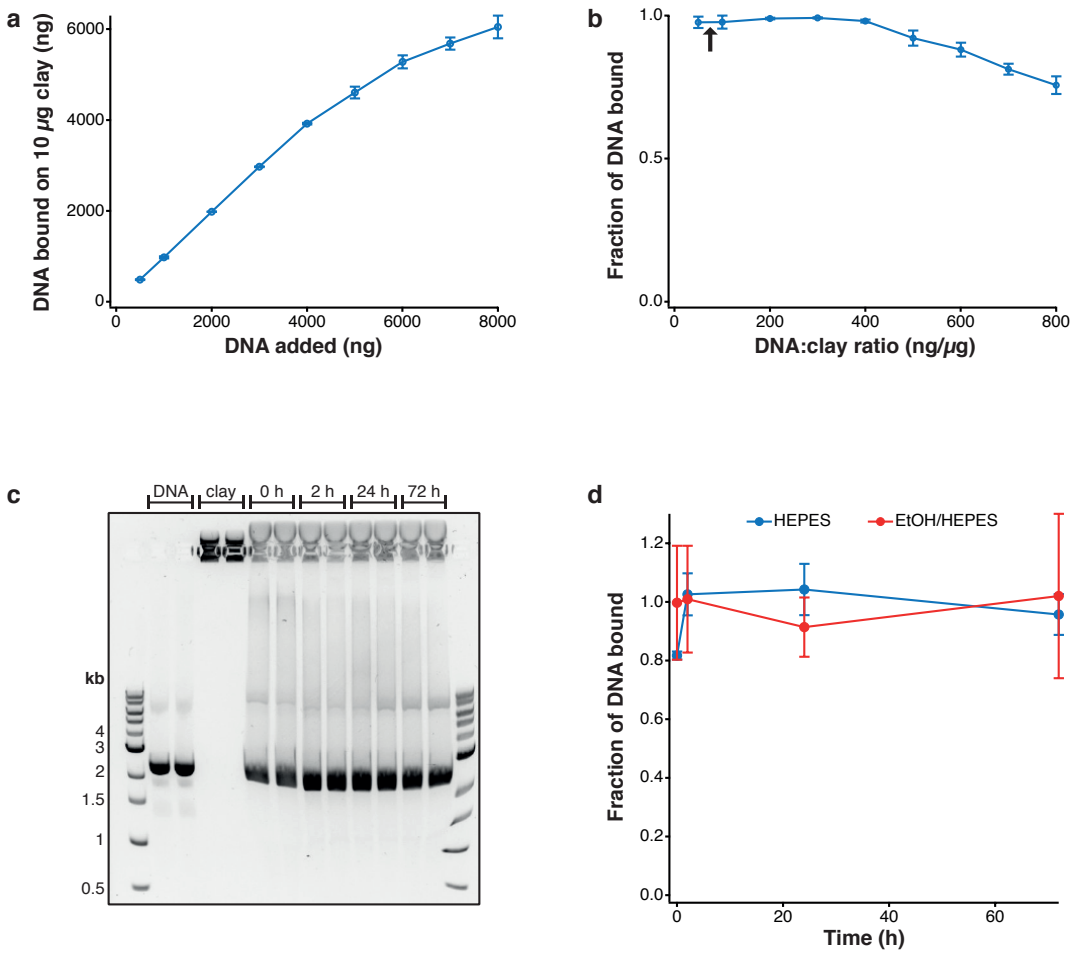

Supplementary Figure S4. Characterization of DNA binding by Laponite XLG clay outside of cell-mimics.

a) Binding curve of plasmid DNA on 10 µg clay. b) Fraction of DNA bound calculated from the same experiment. In cell-mimics, we used DNA at a maximum of 75 ng per µg clay as indicated by the arrow. Binding was measured by titrating plasmid DNA added to 10 µg of Laponite XLG in solution. Hydrogel formation was induced by addition of 200 mM KCl to a final volume of 10 µl. Hydrogel was removed by centrifugation and the DNA left in solution was measured photometrically. Binding experiments were performed in triplicates. Error bars show the standard deviation of the experimental repeats. c, d) Agarose gel analysis of DNA capture and retention under nucleus-formation and cell-mimic storage conditions. Clay-DNA hydrogel was formed at a ratio of 75 ng plasmid DNA per µg clay in 70% ethanol and 200 mM HEPES pH 8. Clay-DNA pellets were stored either in 150 µl 100 mM HEPES pH 8 or in 150 µl 70% ethanol, 200 mM HEPES pH 8 at 4°C for different times to analyze retention of DNA in the hydrogel. Before analysis on an agarose gel, supernatants were removed and hydrogel pellets homogenized. Experiments were performed in duplicate, and each sample was analyzed on two separate gels. c) Example gel for storage in HEPES buffer. The first four lanes were loaded with DNA or clay only. Each lane contained 4 µg clay and 300 ng plasmid DNA. d) DNA amounts in the samples were determined from band intensities on the gel. Error bars are standard deviations of experimental repeats.

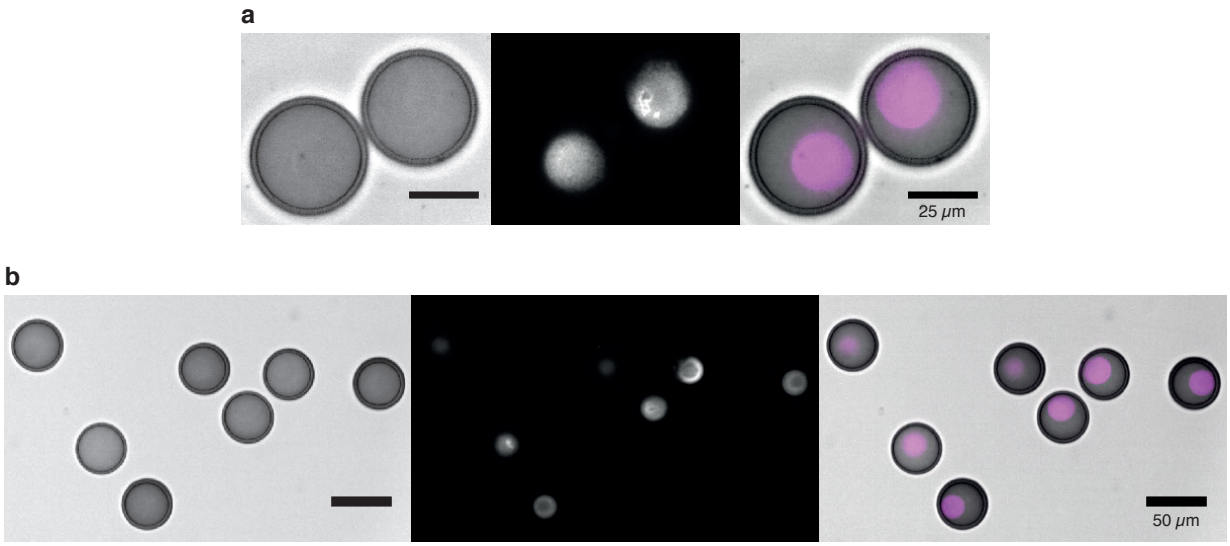

Supplementary Figure S5. Morphologies of clay-DNA nuclei.
a) Examples of clay-DNA hydrogel nuclei morphologies. Shown is a brightfield image (left), GelRed fluorescence of the clay-DNA nucleus (center) and a merged image (left). b) Variability of GelRed fluorescence in hydrogel nuclei. Intensity of dim hydrogel nuclei did not increase by focusing on a different section in cell-mimics.

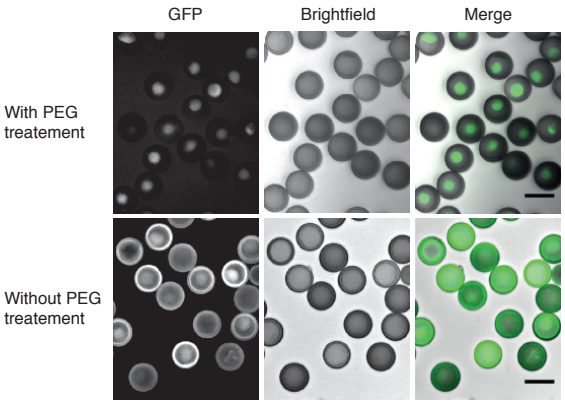

Supplementary Figure S6. PEG treatment prevents non-specific binding of proteins to polymer membranes of cell-mimics.
Endpoint fluorescence of *tetR*-sfGFP / *tetO* cell-mimics (Fig. 1c) and localization of TetR-sfGFP after 3 h TX-TL with or without PEG treatment.

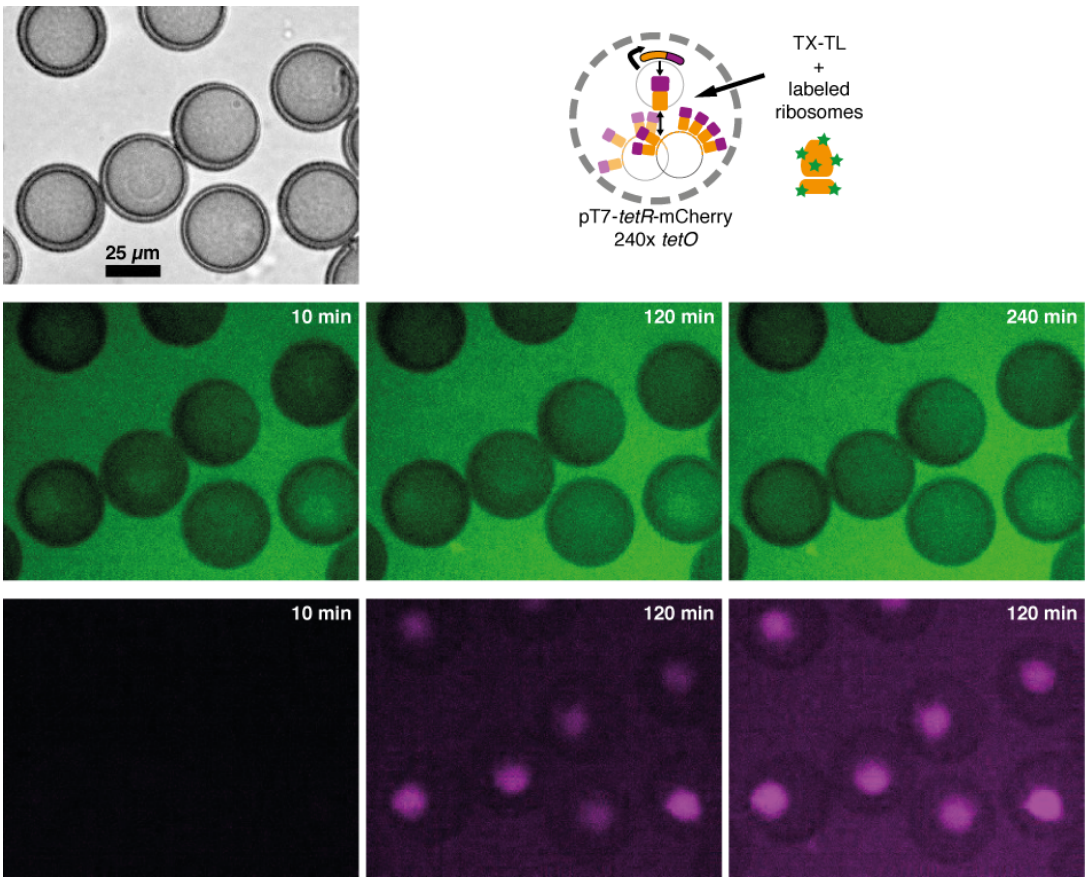

Supplementary Figure S7. Cell-mimics' porous polymer membranes are permeable to ribosomes.
Protein expression in *tetR*-mCherry / *tetO* cell-mimics was initiated by addition of TX-TL reagents spiked with Alexa Fluor 488 labeled *E. coli* ribosomes. Top shows a brightfield image and a schematic of the experiment. Alexa Fluor 488 labeled ribosomes (middle, green) could be detected in cell-mimics interior and in many cell-mimics their concentration was slightly increased in hydrogel nuclei over the rest of the interior. Hydrogel nuclei accumulated TetR-mCherry fluorescence over time (bottom, magenta).

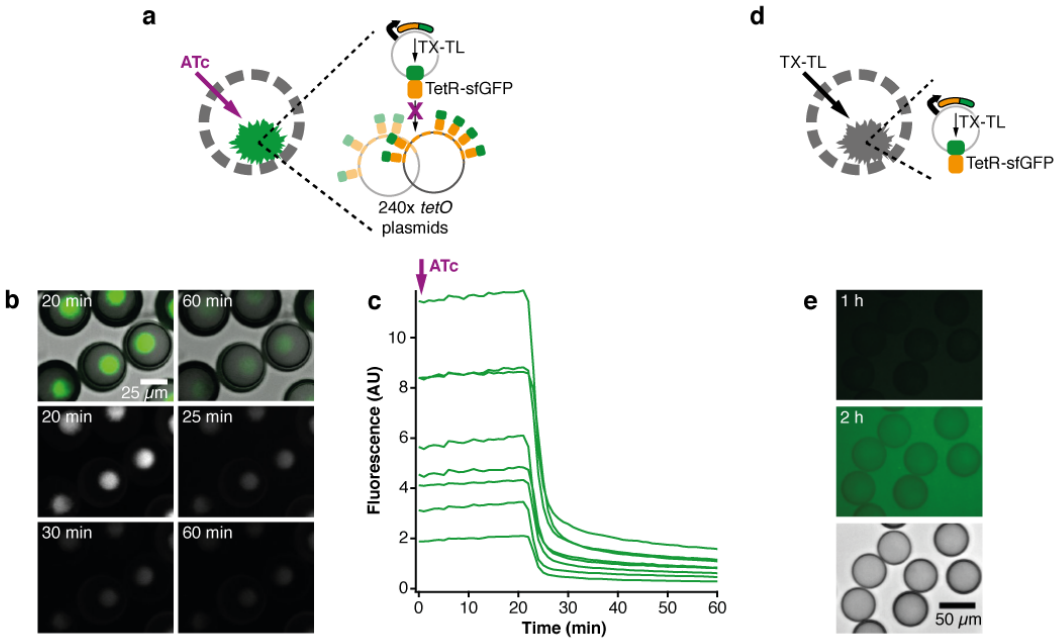

Supplementary Figure S8. Specificity of TetR-sfGFP binding to *tetO* sites in hydrogel nuclei.

a-c) Anhydrotetracycline (ATc) induced unbinding from hydrogel nuclei containing 240x *tetO* plasmid. a) Schematic of the experiment. TetR-sfGFP was expressed in cell-mimics in TX-TL as in Fig. 1d. When expression ended after 3 h, cell-mimics were transferred into 200 mM HEPES pH 8, 2 mg/ml BSA. To observe ATc induced unbinding from nuclei, cells in 18 µl of buffer were pipetted into a cylindrical reaction chamber prepared by punching a 2 mm hole into a 10 mm high block of PDMS, which was placed on cover glass for imaging. ATc for a final concentration of 2.5 µM was pipetted on top of the liquid without active mixing. Imaging was started immediately and ATc was left to diffuse to cell-mimics. b) Timelapse images of TetR-sfGFP unbinding. Shown are merged images before and after unbinding (top) and GFP fluorescence images of the fast disappearance of TetR-sfGFP from hydrogel nuclei. c) Dynamics of the unbinding process observed by tracking fluorescence in several hydrogel nuclei over time. d) Schematic of control experiment of *tetR*-sfGFP expression in cells without 240x *tetO* array plasmid. e) Timelapse images of GFP fluorescence (top, middle). To show increase of fluorescence in solution, images were set to a higher brightness than images in panel b. Bottom: brightfield channel.

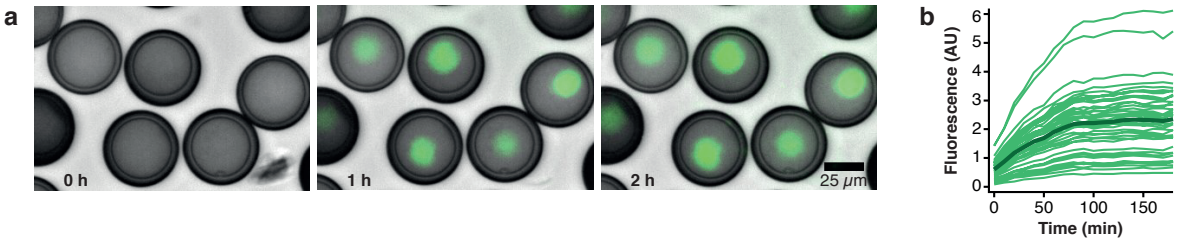

Supplementary Figure S9. Low batch-to-batch variability of protein expression in cell-mimics.
Expression and capture of TetR-sfGFP in a batch of cell-mimics prepared approximately a year later than those shown in Fig. 1. Timelapse images of TetR-sfGFP fluorescence increase in nuclei (green fluorescence merged with brightfield) and b) traces of fluorescence increase in 40 nuclei and averaged fluorescence (bold line).

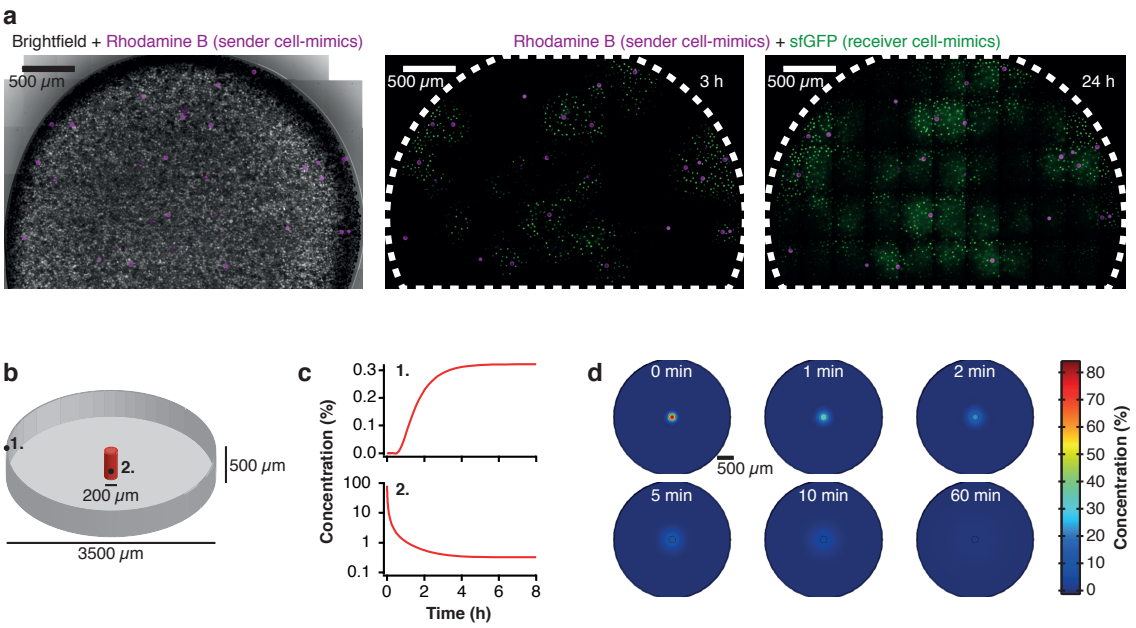

Supplementary Figure S10. Protein exchange in a large droplet of sender and receiver cell-mimics.

a) Brightfield image of dense sender and receiver cell-mimic colony shown in Fig. 2b, merged with fluorescence form sender cell-mimics (magenta). Distribution of TetR-sfGFP fluorescence (green) is shown after 3 h and 24 h with identical brightness settings. b-d) COMSOL simulation of free diffusion of TetR-sfGFP (50.1kDa) in a geometry comparable to the experiment in a). We assumed a diffusion coefficient of $6*10^{-7}$ cm^2 s^{-1}, which was measured for 67 kDa bovine serum albumin (*23*). b) Schematic and dimensions of the geometry used in the simulation. Protein was initially located in a cylindrical region (red) in the center. Protein could freely diffuse in the entire grey cylinder, which was closed on the top and bottom. c) Concentration change in the two positions indicated in b). d) Surface concentration across the geometry at different time points.

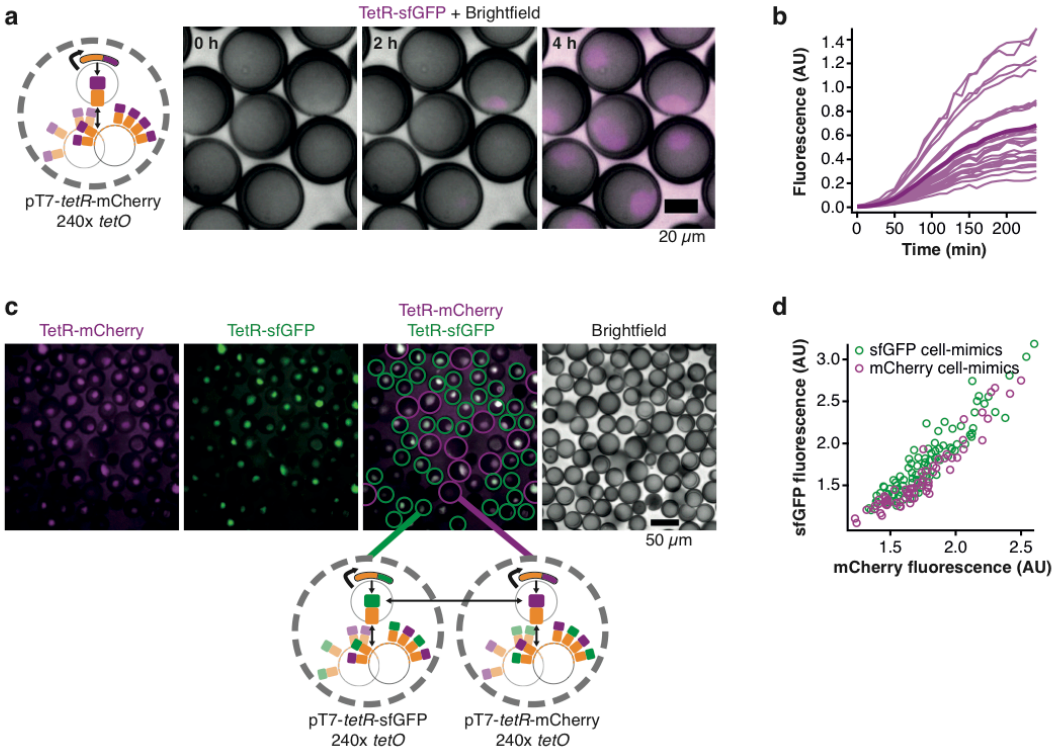

Supplementary Figure S11. Protein exchange between TetR-mCherry and TetR-sfGFP producers.

a) Schematic of cell-mimics expressing and binding TetR-mCherry (*tetR*-mCherry / *tetO*) and time lapse images of TetR-mCherry fluorescence (magenta) merged with brightfield images. b) Traces of fluorescence increase in hydrogel nuclei of 27 *tetR*-mCherry / *tetO* cell-mimics with the average in bold. c) Endpoint fluorescence (4 h) in a mix of *tetR*-sfGFP / *tetO* and *tetR*-mCherry / *tetO* cell-mimics. As shown in the schematic below, both cell-mimics types contain the 240x *tetO* plasmid and bind a mix of both fluorescent reporter proteins. Images show fluorescence channels separately and a merge of both fluorescence channels with circles indicating the positions of TetR-sfGFP producers (green) and TetR-mCherry producers (magenta), which were identified from the brightfield image by their difference in size and cell wall thickness. d) Correlation of sfGFP and mCherry fluorescence in TetR-sfGFP producers (green) and TetR-mCherry producers (magenta). Each data point shows sfGFP and mCherry fluorescence in the hydrogel nucleus of an individual cell-mimic. The cell-mimic types cannot be distinguished from each other by their respective fluorescence levels. Cell-mimics that could not be classified into a category based on their appearance in the brightfield channel were not analyzed.

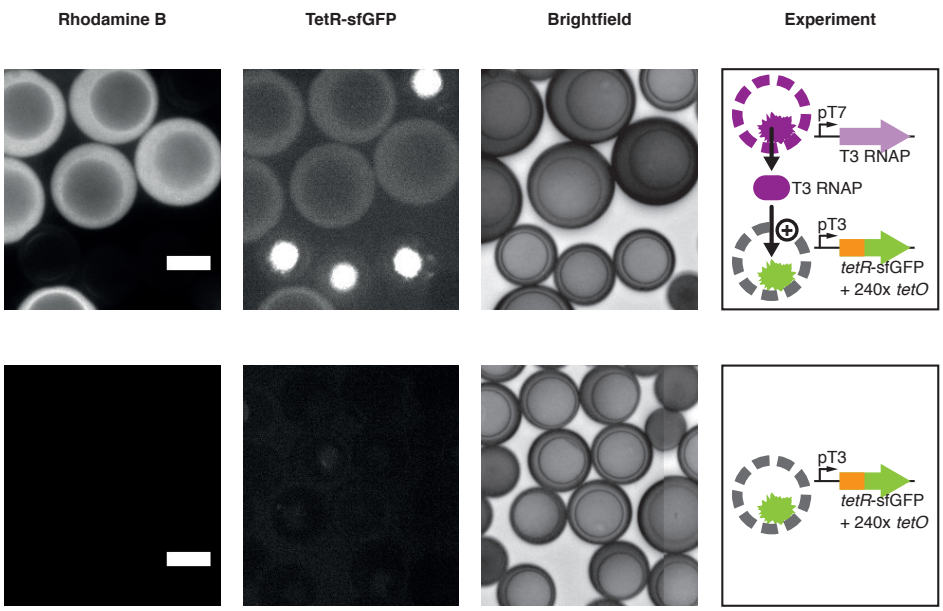

Supplementary Figure S12. Activation of reporter cell-mimics by T3 RNAP producing activator cell-mimics and control experiment.
Images of endpoint fluorescence (3 h) and brightfield channel from activation experiment with a mix of activator and reporter cell-mimics as well as a control experiment using reporter cell-mimics only as shown in the schematic. Activator cell-mimics were labeled with Rhodamine B in their polymer membranes.

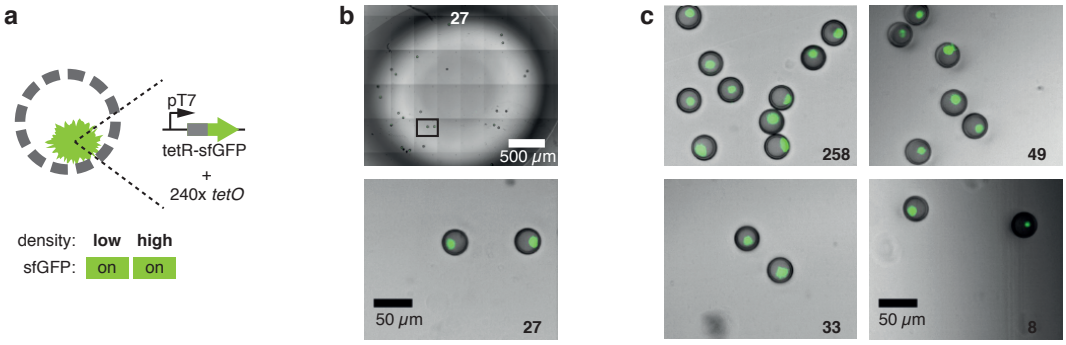

Supplementary Figure S13. Constitutive producers of TetR-sfGFP show the reporter protein in their hydrogel nuclei at low cell-mimic densities.
a) Schematic of control cell-mimics for the artificial quorum sensing experiments (Fig. 4) that express the reporter protein under control of a constitutive T7 promoter and contain the 240x *tetO* plasmid. Independent of cell density, control cells accumulated reporter protein in their nuclei. Constitutively expressing *tetR*-sfGFP / *tetO* control cell-mimics cell-mimics were as in Fig. 1C-D. b) Experiments were performed like in Fig. 4 in droplets of 4.5 µl TX-TL containing different numbers of control cell-mimics as indicated. Lower image is a magnification of the region highlighted above. c) Magnifications of representative control cells in droplets containing the indicated number of cells. All images were set to identical brightness settings.

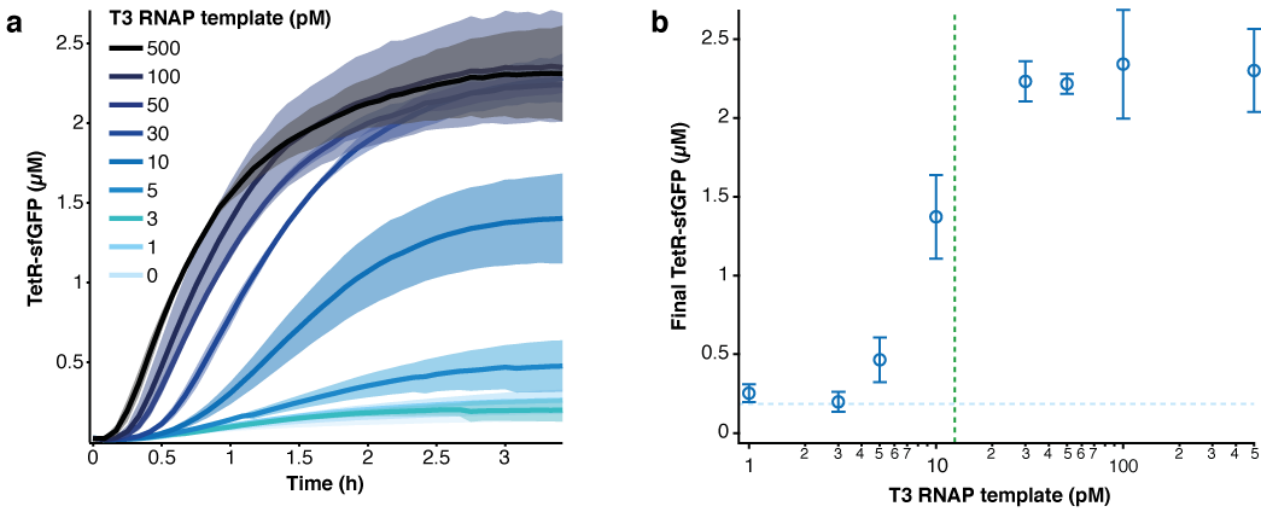

Supplementary Figure S14. Titration of T3 RNAP template DNA in batch reactions.
a) Dynamics of TetR-sfGFP production from a T3 promoter in TX-TL reactions containing different amounts of T3 RNAP template DNA. GFP fluorescence was read on a platereader in reactions containing 5 nM pT3-tetR-sfGFP reporter plasmid and variable amounts of pT7-T3RNAP linear template DNA. All reactions were done at least in triplicate and shaded areas indicate standard deviations between experimental repeats. b) Final TetR-sfGFP produced in a) as a function of T3 RNAP template concentration. Light blue dashed line indicates fluorescence of a reaction with no T3 RNAP template. Green dashed line indicates calculated T3 RNAP template concentration in a 4.5 µl droplet containing 400 artificial quorum sensing cell-mimics, which was the lowest density at which expression of the reporter was observed in Fig. 4c.

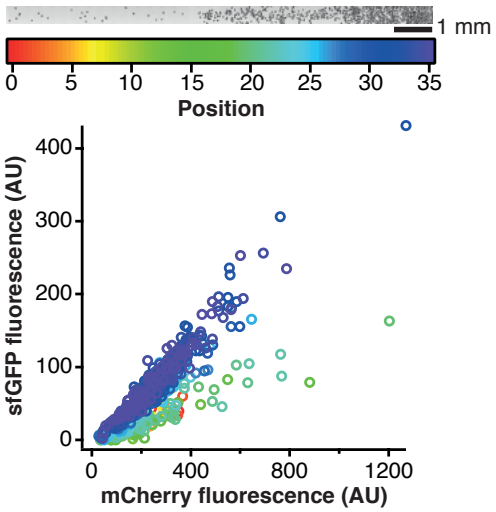

Supplementary Figure S15. Crowded and dilute 2-color density sensors display sfGFP to mCherry fluorescence in two distinct populations.
Fluorescence of individual cell-mimics in the density gradient experiment shown in Fig. 4e is plotted as sfGFP versus mCherry fluorescence. Positions of individual cell-mimics in the gradient are color coded as shown in the color legend and the corresponding image above.

Table S1. DNA templates used in this study

Name	Function	Description	Reference
240x *tetO* array	Array of 240 TetR binding sites (*tetO*), PRS316-240xtetO (Addgene #44755)	Plasmid, high copy number, Ampicillin	(*24*)
pT7-*tetR*-sfGFP	T7 promoter driven synthesis of C-terminal fusion of sfGFP to TetR repressor (TetR-sfGFP)	Plasmid, pTNT vector (Promega), high copy number, Ampicillin	This work
pT7-*tetR*-mCherry	T7 promoter driven synthesis of TetR-mCherry fusion protein	Plasmid, pTNT vector (Promega), high copy number, Ampicillin	This work
pT3- *tetR*-sfGFP	T7 promoter driven synthesis of TetR-sfGFP	Plasmid, pSB1C3 (Registry of Standard Biological Parts), high copy number, Chloramphenicol	This work
pT7-T3RNAP	T7 promoter driven synthesis of T3 RNA polymerase (only used as PCR template)	Plasmid, Low copy number, pSC101 origin, Kanamycin	This work
pT7-T3RNAP	T7 promoter driven synthesis of T3 RNA polymerase	Linear DNA, PCR amplification of functional region from pT7-T3RNAP plasmid	This work

Table S2. DNA content of cell-mimics used in this study. Listed are DNA concentrations used in inner aqueous phase for double emulsion production.

Name and Description	**DNA concentrations**
tetR-sfGFP / *tetO* Production and capture of TetR-sfGFP	50 nM pT7_*tetR*-sfGFP plasmid 20 nM 240x *tetO* array plasmid
tetR-mCherry / *tetO* Production and capture of TetR-mCherry	50 nM pT7_*tetR*-mCherry plasmid 20 nM 240x *tetO* array plasmid
Sender cell-mimics Production of TetR-sfGFP	100 nM pT7_*tetR*-sfGFP plasmid
Receiver cell-mimics Capture of TetR-sfGFP	20 nM 240x *tetO* array plasmid
Activator cell-mimics Production of T3 RNAP	40 nM pT7_T3RNAP linear DNA
Reporter cell-mimics T3 promoter controlled production and capture of TetR-sfGFP	30 nM pT3_*tetR*-sfGFP plasmid 20 nM 240x *tetO* array plasmid
1-color density sensors cell-mimics Artificial quorum sensing	2.5 nM pT7_T3RNAP linear DNA 30 nM pT3_*tetR*-sfGFP plasmid 15 nM 240x *tetO* array plasmid
2-color density sensor cell-mimics Artificial quorum sensing with 2-color response	2.5 nM pT7_T3RNAP linear DNA 20 nM pT3_*tetR*-sfGFP plasmid 20 nM pT7_*tetR*-mCherry plasmid 15 nM 240x *tetO* array plasmid

Movie 1. Production of double emulsion droplets.
Timelapse movie of the formation of water-in-oil-in-water emulsion droplets for the production of artificial cell-mimics with hydrogel nuclei. Some inhomogeneity can be observed in droplet sizes and breakage of droplets that results in polymer beads after polymerization. Flow rates were 300 µl/h for the outer aqueous, 40 µl/h for the middle organic and 12 µl/h for the inner aqueous phase.

Movie 2. Expression and capture of TetR-sfGFP in hydrogel nuclei of cell-mimics.
Timelapse movie of the expression of TetR-sfGFP in cell-mimics containing pT7-*tetR*-sfGFP expression and 240x *tetO* array plasmids (see Fig. 1). Merge of brightfield channel and sfGFP fluorescence (green).

Movie 3. Communication between cell-mimics via a diffusive genetic activator signal.
Activation of gene expression from T3 RNAP producing activator cell-mimics (magenta) to reporter cell-mimics (see Fig. 3). Merge of brightfield channel, sfGFP fluorescence (green) and rhodamine B fluorescence (magenta).